2021 43rd Annual International Conference of the
IEEE Engineering in Medicine & Biology Society (EMBC)
Oct 31 - Nov 4, 2021. Virtual Conference

3D Cardiac Computational Model for Evaluating the Progression of Myocardial Ischemia in a Supply-Demand Paradigm

Oishee Mazumder[1], Dibyendu Roy[1], Sundeep Khandelwal[1] and Aniruddha Sinha[1]

Abstract— **In this paper, we present a cardiac computational framework aimed at simulating the effects of ischemia on cardiac potentials and hemodynamics. Proposed cardiac model uses an image based pipeline for modeling and analysis of the ischemic condition in-silico. We compute epicardial potential as well as body surface potential (BSP) for acute ischemic conditions based on data from animal model while varying both local coronary supply and global metabolic demand. Single lead ECG equivalent signal processed from computed BSP is used to drive a lumped hemodynamic model and derive left ventricular dynamics. Computational framework combining 3d structural information from image data and integrating electrophysiology and hemodynamics functionality is aimed to evaluate additional cardiac markers along with conventional electrical markers visible during acute ischemia and give a broader understanding of ischemic manifestation leading to pathophysiological changes. Simulation of epicardial to bodysurface potential followed by estimation of hemodynamic parameters like ejection fraction, contractility, blood pressure, etc, would help to infer subtle changes detectable beyond conventional ST segment changes.**

I. Introduction

Myocardial ischemia (MI) is caused due to insufficient blood flow in some regions of myocardium leading to decreased oxygen supply. Imbalance between myocardial oxygen supply and demand dictates the pathophysiological manifestation of the disease [1]. Clinical marker for MI are changes observed in electrocardiogram (ECG), caused due to shifts in ionic concentration related with oxygen deficiency [2]. An apparent shift of ST segment occurs depending on extent of ischemia, and can be localized through specific leads of ECG that shows ST segment elevation or depression. Although ST segment shifts provides an estimate of ischemic behavior, mostly in transmural ischemic cases, its effectiveness and reliability as a marker for non-transmural ischemia has been long debated. The ability of ST depression to locate ischemia is considered much less specific, with average accuracy rates ranging from 68-75% [3]. As MI is predominantly initiated due to supply-demand imbalance, a clear understanding of the hemodynamic changes involved in the pathophysiological process responsible for genesis of MI is essential for its evaluation along with ST segment changes [4].

The biophysical basis for ECG evaluation of MI is based on the notion of endocardial origin of intramural injury currents that lead to ST segment deflections within ECG recordings. Recent studies using animal models have emphasized on a more distributed ischemic growth pattern throughout the myocardial wall, thus questioning the foundation of ischemic progression analysis through ST depressions [5]. An alternative to extensive animal experimental procedures to study ischemic effect is through in-silico cardiac computational models [6]-[7]. Bulk of these models compute ischemic effect through singular, subendocardial ischemic zones, using cardiac volume conductor as a source to generate extracellular potential [8]-[9].

Existing computational model on replicating the electrical effects of ischemia concentrates more on distribution of the extra-cellular potential and ischemic border zone dynamics [10]-[11]. The effect of ischemic injury current on body surface potential and its manifestation in form of conventional ECG readings are neither simulated or addressed. Another major drawback of in-silico cardiac models simulating ischemic effect lies in the fact that these models predominantly simulates only the electrophysiological (EP) changes, completely omitting the effect of hemodynamics and autoregulatory mechanisms. Ischemic effects compromises myocardial contractility, leading to pump inefficiency and heart failure [12]. These changes are expressed through variations in cardiac hemodynamic parameters. Cardiac computational models integrating the dual aspect of EP and hemodynamics are required to understand and predict ischemic progression leading to heart failure.

Motivated by the limitations in current cardiac in-silico models in manifesting ischemic dynamics, we aim to create a 3D cardiac computational model, coupling the effect of electrophysiology (EP) and hemodynamics. The proposed model would aid to create a deeper understanding on the pathophysiological manifestation of MI, starting from its inception in myocardial tissue to its effect in Body surface potential (BSP) variation, along with its effect on left ventricle dynamics, translated to pumping function of heart.

Proposed cardiac computational model consists of a 3D cardiac structure, computed from MRI slices through segmentation and meshing and finite element methods to compute extracellular and epicardial potential in ischemic condition using experimental torso-tank data of a canine [13]. Forward EP is implemented using a Bi-domain source model and is used to compute BSP and a single lead ECG equivalent from epicardial potential distribution. The simulated ECG from the EP framework is used to drive the lumped hemodynamic model, consisting of 4 chambered heart with pulmonic and systemic circulation, capable of capturing the pressure volume dynamics of all the cardiac chambers for each and every phase of cardiac cycle. We compute EP and

[1]Oishee Mazumder, Dibyendu Roy, Sundeep Khandelwal and Aniruddha Sinha are with TCS Research, Tata Consultancy Services Ltd, India.
Email:oishee.mazumder@tcs.com, dibyendu.roy@tcs.com, sundeep.khandelwal@tcs.com, aniruddha.s@tcs.com

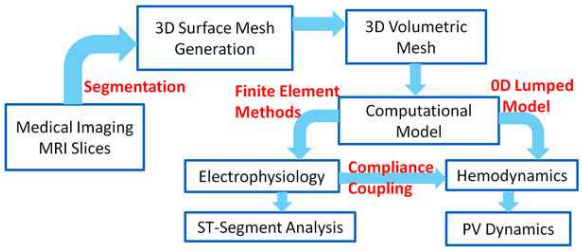

Fig. 1: Schematic of the cardiac computational model functional blocks

hemodynamic parameters for a series of acute ischemia by varying both local coronary supply and global metabolic demand, giving rise to two specific ischemic group, naming 'Supply ischemia' and 'Demand ischemia'.

II. Methodology

The workflow for the proposed cardiac model is two fold, highlighted below:

- 3D cardiac computational model to compute cardiac potential distribution during Supply and Demand Ischemia
- Simulation of BSP and coupling of the computational model with hemodynamic model to derive pressure-volume dynamics

For the 3D cardiac modeling pipleline, we created a volume conductor model of an ischemic heart based on Utah torso tank data. The MR images of the heart were derived from a canine heart that was scanned to obtain anatomy, fiber orientation and the perfusion bed of left anterior descending (LAD) artery. For experimental studies, canine heart is often used as a substitute of human heart due to the close similarity in conduction system [14]. From these MR slices, extra-cellular cardiac potentials were estimated. For linking hemodynamics functionality, first, BSP were derived using extra-cellular cardiac potential and subsequently, the single lead ECG equivalent was used to drive the hemodynamic module. Work-flow schematic of the developed model is shown in Fig.1.

A. Torso Tank data

Imaging data along with geometry information for meshing and conductivity were used from the 'double dog experiment' data [13] and is summarized in brief. The experiment described was performed under deep anesthesia, where an isolated heart from one dog was perfused via blood from the support dog. LAD region of the isolated heart was cannulated and occluded. A pacing clip in right ventricle provided heart rate control. Epicardial potential were recorded using a 247-electrode epicardial sock along with 40 intramural needle electrode around the occluded LAD section. The isolated, perfused heart was suspended in a human torso shaped tank with 192 electrodes and filled with an electrolytic solution.

The study protocol was designed to vary the supply-demand equilibrium by combining elevated heart rate (demand) and reduced coronary flow (supply) in different combination. Out of the complete data-set, we have utilized a particular set of supply and demand variation; Supply variation from 20ml/min to 5 ml/min in four consecutive experiments, decreasing the flow rate in steps of 5 ml/min with a fixed pacing rate of 350 ms (S_1, S_2, S_3, S_4). Four similar demand experiment at 15 ml/min fixed flow, varying pacing rate from 350 ms to 275 ms, at step of 25 ms per experiment (D_1, D_2, D_3, D_4). For each supply and demand experiment, reading were taken for an occlusion cycle of 180 sec, spanned in to three consecutive reading at initiation (0 sec), 90 sec and 180 sec. In total there are 12 individual experimental runs for each supply and demand group along with their respective control(c) run. Control for both supply and demand had flow of 35ml/min.

B. 3D Computational model

Computational pipeline leading to 3d cardiac model comprises of segmenting the MRI scans to extract area of interest (ventricular section with occlusion) using Seg3D [15] followed by volumetric mesh generation using BioMesh3D [16]. DW-MRI images from the dataset were used to define principal eigenvectors associated with each voxel within the heart volume, which corresponded to fiber orientation within the heart, used to compute anisotropic conductivity tensors. Bidomain model implementation to derive extracellular potential, forward EP computation and visualization were all done in SCIRun enviorenment [17].

Extracellular and epicardial potential inherent to ischemic condition is modulated through generation and propagation of injury currents. In order to model these currents to simulate the effect of ischemia, description of the electrical properties of both the intracellular and extracellular spaces are required. These spaces can be modeled as anisotropic volume conductors having the shape of heart and anisotropy caused by fiber structure of the myocardium. The governing partial differential equations to solve in both spaces are [11]: $\nabla.\Sigma_i\nabla\phi_i = i_{mem}$; $\nabla.\Sigma_e\nabla\phi_e = -i_{mem}$ where, ϕ_i and ϕ_e are the intracellular and extracellular potentials, Σ_i, and Σ_e are the conductivity tensors of both spaces and i_{mem} is the current through the membrane. Net transmembrane potential (TMP) can be defined as: $V_m = \phi_i - \phi_e$. Combining the TMP and membrane current equations results in defining extracellular potential as a function of TMP (V_m): $\nabla.(\Sigma_i + \Sigma_e)\nabla\phi_e = -\nabla.\Sigma_i\nabla V_m$.

To solve for a specific heart, description of Σ_i and Σ_e as a function of space along with description of how V_m changes throughout the ischemic zone is required. These constraints are set using Neumann boundary condition along the epicardial surface and Cauchy boundary conditions along the endocardium, expressed as:

$$\begin{aligned} \overrightarrow{n}_{epi}.(\Sigma_e+\Sigma_i)\nabla\phi_e = 0 \quad & x \in \partial\Omega_{M,epi} \\ \overrightarrow{n}_{endo}.(\Sigma_e\nabla\phi_e) = \overrightarrow{n}_{endo}.(\Sigma_b\nabla\phi_b) \quad & x \in \partial\Omega_{M,endo} \\ \phi_e = \phi_b \quad & x \in \partial\Omega_{M,endo} \\ \phi_i = 0 \quad & x \in \Omega_b \end{aligned} \tag{1}$$

where, ϕ_e and ϕ_b are the potentials within the extracellular cardiac tissue and blood domains, respectively, and Ω_M represents the cardiac volume, which is bounded by the

epicardial $(\partial\Omega_M, epi)$ and endocardial$(\partial\Omega_M, endo)$ surfaces with their respective surface normal unit vectors $\overrightarrow{n}_{epi}$ and $\overrightarrow{n}_{endo}$. Conductivity tensor were extracted from DTI images by decomposition of the tensor from fiber orientation and extracting the dominant direction. The resulting volume conductor equation was solved using Galerkin method, reducing it to a finite element weak PDE form, computed in SCI environment.

C. Forward EP and BSP generation

EP model largely comprises of solving the forward problem, i.e, calculating body surface potential from a known heart potential [18]. The general simulation framework is similar to the volume conductor model and bidomain simulation used to generate extracellular potential in previous section. The governing equation in forward EP is the modified steady state electrical potential in an in-homogeneous volume conductor described by Laplace equation: $\nabla.(\sigma\nabla\phi) = 0$, where, σ is the conductivity tensor field and ϕ is the electric potential. This is subjected to Dirichlet boundary condition $(\phi(x,y,z)\mid_{\Omega_k} = V_k)$, applied anywhere the electric potential is known and Neumann boundary conditions $(\frac{\partial\phi}{\partial n}\mid_{\Omega} = 0)$ applied on the surface of the object being simulated. $V_k$is the known potential of electrode k (placed at torso), and Ω_k specifies the domain coincident with electrode k placed at the torso.

FEM applied in this volume model begins by subdividing the geometry into a set of volume elements with vertices at a set of nodes, and then approximating the potential in the volume by a basis expansion: $\bar{\phi}(x,y,z) = \sum \phi_i N_i(x,y,z)$, where N_i are a set of basis functions, one for each node in the volume element discretization, and ϕ_i are the corresponding coeffcients at those nodes. This is solved using SCIRun enviorenment [19]. Human torso geometry data were obtained from a dataset developed by SCI Institutes NIH/NIGMS CIBC Center [20]. 192 tank electrode data were imposed on the torso model to form a computational mesh. Torso images were segmented based on the major organs in the torso with tissue conductivity values as specified in literature [21].

Fig.2 shows an instance of simulated cardiac and torso potential at ventricular repolarization phase (precisely ST segment at 40%), for one particular supply and demand condition along with the control non-ischemic simulation. As evident in the figure, for ischemic simulation, due to the generation of ischemic current, potential distribution at both epicardial and torso surfaces shows increased potential gradient compared to the non-ischemic control part. From the resultant BSP expressed as potentials recorded at 192 locations, single lead ECG signal corresponding roughly to Lead V location was used in successive computations.

D. Hemodynamic Coupling

Hemodynamic model consists of a four chambered heart with systemic and pulmonic circulation along baroreflex auto-regulation, described earlier in [22]. Coupling of EP and hemodynamics block is through a compliance function, which determines the time-varying compliance of auricles and ventricle and brings about the pumping action of the heart [23]. Single lead ECG signal (Fig.2) can be decomposed based on features like peak amplitudes and corresponding cardiac cycle time of major events like ventricular depolarization, repolarization, etc. As shown in Fig.2, PQRST events are expressed as in generic ECG signal for one cardiac cycle $\left[(A_P,t_P)\ \ (A_Q,t_Q)\ \ (A_R,t_R)\ \ (A_S,t_S)\ \ (A_T,t_T)\right]$ respectively. These amplitude and time stamps are used to map time-varying compliance functions for the cardiac chambers. Compliance function for ventricles (C_{lv}, and C_{rv}) are expressed as:

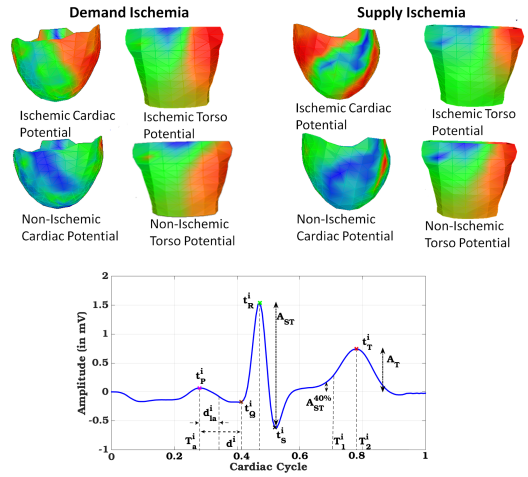

Fig. 2: Simulated cardiac and torso potential for Ischemic and non-Ischemic conditions along with Single lead representative ECG

$$C_i(t) = C_i \times u_v(t-d), \quad i \in \{lv, rv\} \tag{2}$$

$$u_v(t) = \begin{cases} 0.5 - 0.5\cos\left(\pi\frac{t}{T_1}\right), & 0 \le t < T_1 \\ 0.5 + 0.5\cos\left(\pi\frac{t-T_1}{T_2-T_1}\right), & T_1 \le t < T_2 \\ 0, & T_2 \le t < T \end{cases} \tag{3}$$

where $u_v(t)$ is the activation function, and $d = (t_R - t_P)$ represents the delay in activation of ventricles, $T_1 = (T_r + T_t)/2$ and $T_2 = T_t$ are the systolic and diastolic duration of the cardiac cycle (T) respectively. The ventricular-compliance $(C_i; \forall i \in \{lv, rv\})$ are computed by the ratio between the R-peak and T-peak ($C_i = \frac{A_R}{A_T}$).

From the hemodynamic model, parameters like mean arterial pressure (MAP), complete dynamics of left ventricle (LV), cardiac output (CO), stroke volume (SV), ejection fraction (EF), end systolic, end diastolic pressure, volume (ESP, EDP, ESV, EDV) and their respective ratio (ESPVR, EDPVR) can be calculated which reveals concise information related to the state of heart and cardiovascular system.

III. Result and Discussion

Using the developed computational model, we simulated BSP and lead V equivalent ECG for the 12 different supply and demand ischemia setup along with the control condition and derived hemodynamic parameters associated with generic LV functioning. Fig.3 shows the simulated ECG

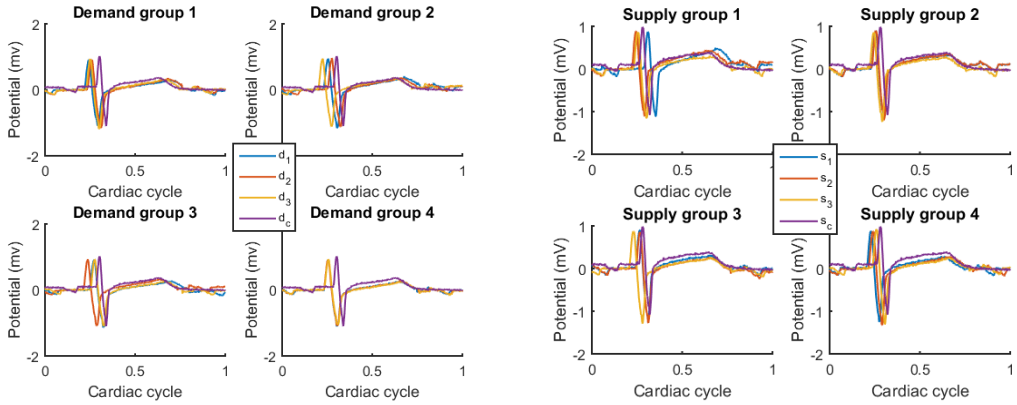

Fig. 3: Simulated single lead ECG for Demand and Supply ischemia runs

TABLE I: Cardiac parameters for Supply-Demand ischemic runs

Condition	δST	HR	RPP	EF	ESPVR	EDPVR	Condition	δST	HR	RPP	EF	ESPVR	EDPVR
$Demand_{1,1}$	0.0714	136.36	215.03	39.23	0.0829	1.9969	$Supply_{1,1}$	0.0334	117.6	173.28	43.2	0.0815	1.9776
$Demand_{1,2}$	0.0652	133.92	209.25	39.74	0.0802	2.0048	$Supply_{1,2}$	0.0269	128.20	198.58	40.67	0.0810	1.9854
$Demand_{1,3}$	0.0676	130.43	201.38	40.23	0.0864	1.9963	$Supply_{1,3}$	0.0551	132.15	206.49	39.95	0.0878	1.9929
$Demand_{2,1}$	0.0437	135.4	212.82	39.39	0.0801	2.0025	$Supply_{2,1}$	0.0435	127.65	197.11	40.8	0.0810	1.9985
$Demand_{2,2}$	0.0354	124.48	188.93	41.60	0.0814	1.9869	$Supply_{2,2}$	0.0393	127.38	196.35	40.87	0.0810	1.9796
$Demand_{2,3}$	0.0469	130.43	205.32	40.00	0.0910	2.0042	$Supply_{2,3}$	0.0596	129.03	201.37	40.46	0.0814	1.9920
$Demand_{3,1}$	0.0706	138.89	220.27	38.91	0.0799	2.0045	$Supply_{3,1}$	0.0528	127.38	195.29	40.87	0.0817	1.9837
$Demand_{3,2}$	0.0556	130.71	204.82	40.06	0.0811	2.0023	$Supply_{3,3}$	0.0878	126.84	194.23	40.93	0.0817	1.9977
$Demand_{3,3}$	0.0817	128.20	197.97	40.82	0.0810	1.9951	$Supply_{3,3}$	0.0903	136.98	217.94	38.93	0.0805	1.9980
$Demand_{4,1}$	0.0858	129.58	202.01	40.40	0.0812	1.9901	$Supply_{4,1}$	0.0831	129.58	202.31	40.72	0.0828	1.9968
$Demand_{4,2}$	0.0866	132.15	206.72	39.93	0.0834	1.9943	$Supply_{4,2}$	0.1021	138.88	205.81	40.61	0.0807	2.0044
$Demand_{4,3}$	0.0885	132.74	207.37	39.89	0.0804	2.0071	$Supply_{4,3}$	0.0978	129.87	221.07	38.48	0.0801	1.9928
$Demand_c$	0	102.73	143.92	46.47	0.0837	1.7921	$Supply_c$	0	106.19	150.51	45.60	0.0826	1.9479

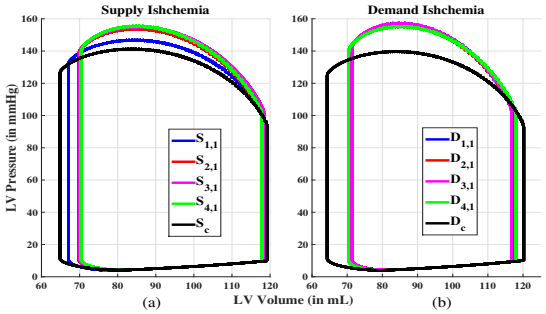

Fig. 4: PV loop for a) Supply conditions; b) Demand conditions

signal for demand and supply group. As evident from the curves, ST segment variation is very limited in all the plots, mainly due nontransmural nature of the ischemia. Hence, only ST segment or even other conventional markers like QRS amplitude or T wave amplitude do not provide meaningful insights or any differentiation between supply group or the demand group. Supply group 1 to 4 had reduced coronary supply from 20ml/min in group 1 to 5 ml/min in group 4. For group 4, ST segments were depressed for all three readings compared to the control data, indicating ischemic behavior. No such confirmatory trend are observed through simulated ECG for the demand groups or the other supply group.

Fig.4 shows the hemodynamic parameter variations across the supply and demand group in form of LV pressure-volume (PV) loop. PV loop holds information related to the cardiac phases and action of the valves during a cardiac cycle. All relevant medical markers like ESV, EDV, ESP, EDP are calculated from PV loop, which is again used to calculate the derived clinical index of EF, SV, contractility and stiffness of myocardial tissues. PV loops were generated for initial cardiac instance (0 sec) for 4 group of demand and supply ischemia against their control. As seen in Fig.4a, for the supply group, a clear gradation with respect to flow constraint is evident in the plot. Group 4 with flow rate of 5 ml/min shows increased ESP and ESV with respect to control and other group, indicating a reduced ejection fraction and compromised LV functionality. For demand cases (Fig.4b), PV loop shrinks for all the groups against the control, indicating an overall reduction in SV and EF. There is also marked increase in systolic pressure, indicating a hypertension trend. Comparing in between groups, as the pacing rate decreases from group 1 to 4, PV loop characteristic slightly shifts towards the control group, trend more prominent for the 4th group with pacing time of 275 ms. Unlike demand group, where distinction between group 1, 2 and 3 are negligible, for the supply group, the effect of reduced flow is more pronounced between groups.

Table I lists all the potential markers derived from our model that could differentiate ischemic progression along

with the conventional ST segment changes. The parameters are change in ST segment amplitude at 40% duration of ST phase wrt control ECG (δST), adjusted Heart rate (HR), rate pressure product (RPP), which is the product of heart rate and systolic BP, EF, ESPVR which correlates with ventricular muscle stiffness and EDPVR correlating with contractility for demand and supply group. Changes in δST do not follow any explainable trend, again pointing out the limitation of ST segment evaluation for non transmural ischemic events. Adjustment in terms of baroreflex autoregulation brings down heart rate despite high pacing rate of initiation. For the demand groups, as pacing rate increases, HR also increases but within the same group, HR is maximum for initial instance (0 sec) and slowly decreases as time progress indicating the regulatory effect of hemodynamical adaptation. For the supply group, with decrease in flow, HR increases, as should be the trend [24]. Product of heart rate and systolic BP are frequently referred to as the most important determinant of myocardial oxygen demand [25]. Higher the value, more intense the ischemic effect. For RPP, Supply group indexes are more consistent compared to the demand counterpart. This is partly due to more pronounced effect of HR in the demand group due to change in autoregulation with changing rate of pacing. EF is the most important index that determines LV pumping functionality and it follows a decreasing trend as ischemic effect increases, correlating with medical trends. Here also, supply group results are more consistent than demand counterpart. In terms of ventricular stiffness index (ESPVR), as ischemia progresses, scar tissue generation makes ventricular walls more stiff, thus reducing the net pumping action. In demand group, ESPVR shows slight variation, mostly prominent at initiation of ischemic event but no specific trend was observed for the supply group, with overall ESPVR remaining almost similar for all group variation. Similarly for EDPVR, variations for both supply and demand group are insignificant. This is mostly due to nontransmural nature and a low to moderate severity of ischemic simulation.

IV. Conclusion

In this paper, we propose a 3D cardiac model involving image based processing pipeline and integrating EP and hemodynamics functionality to study the effect of two ischemic groups, naming supply and demand ischemia. Results indicate that hemodynamic parameters along with EP parameters provide a holistic understanding on the behavior of supply and demand ischemic manifestation. A clear understanding of the hemodynamic changes involved in the pathophysiological process responsible for genesis of MI is essential for understanding disease progression and also in clinical applications like selection of anti ischemic drug or specific therapy for a particular disease type manifestation. Through the insights captured from the developed model, alternative hemodynamic biomarkers can be associated with nontransmural ischemic progression for better characterization of the ischemic region.

References

[1] T.Gaziano, A.Bitton, S.Anand, S.Gessel and A.Murphy,(2010), Growing epidemic of coronary heart disease in low-and middle-income countries. Current problems in cardiology;vol: 35, pp: 72-115.

[2] I.Kubota, M.Yamaki M Tomoike (1993). Role of ATP-sensitive K+ channel on ECG ST segment elevation during a bout of myocardial ischemia. Circulation; vol:88, pp:1845-51.

[3] Gorgels A (2013). ST elevation and non-ST elevation acute coronary syndromes: should the guidelines be changed? J Electrocardiol ; vol:46, pp:318-23.

[4] T.Saito T, Tamura Y, et al (2003). Reduction of ST elevation in repeated coronary occlusion model depends on both altered metabolic response and conduction property. Int J Cardiol;vol:92, pp:219-27.

[5] K Aras, B Burton, D Swenson, R.MacLeod (2016), Spatial organization of acute myocardial ischemia; Journal of Electrocardiology, vol: 49, pp:323-336.

[6] A.Perez, R.Sebastian and J.Ferrero, (2015), Three-dimensional cardiac computational modelling: methods, features and applications; BioMedical Engineering OnLine; 14:35.

[7] B.Rodriguez, N.Trayanova and D.Noble, (2006), Modeling Cardiac Ischemia, Ann N Y Acad Sci.vol:1080,pp:395-414.

[8] K Aras, B Burton, D Swenson, R.MacLeod (2014). Sensitivity of epicardial electrical markers to acute ischemia detection. J Electrocardiol; vol:47, pp:836-41.

[9] A.Ryu, K.Lee, S.Kwon, E.Shin, and E.Shim (2019), In silico evaluation of the acute occlusion effect of coronary artery on cardiac electrophysiology and the body surface potential map; Korean J Physiol Pharmacol;23(1),pp:71-79

[10] B.Burton, K. Aras, W.Good, J.Tate, S. MacLeod (2018); A Framework for Image-Based Modeling of Acute Myocardial Ischemia Using Intramurally Recorded Extracellular Potentials , Ann Biomed Eng; vol: 46(9), pp: 1325-1336.

[11] B.Burton, K. Aras, W.Good, J.Tate, S. MacLeod (2018), Image-Based Modeling of Acute Myocardial Ischemia Using Experimentally Derived Ischemic Zone Source Representations; J Electrocardiol, vol: 51(4), pp:725-733.

[12] R.Bonow, G.Maurer, K.Lee, T.Holly, P.Binkley, (2011), Myocardial viability and survival in ischemic left ventricular dysfunction. N Engl J Med; vol: 364, pp: 1617- 1625.

[13] A. Kedar, MacLeod, Rob et.al (2015). Experimental Data and Geometric Analysis Repository-EDGAR. Journal of electrocardiology. 48; https://www.ecg-imaging.org/edgar-database

[14] H.Smith, Hurley P et.al (1975). Changes in myocardial blood flow and ST segment elevation following coronary artery occlusion in dogs. Circulation Research; vol 36, pp:697-705.

[15] CIBC. Seg3D: Volumetric Image Segmentation and Visualization. Scientific Computing and Imaging Institute (SCI). http://www.seg3d.org.

[16] M.Callahan M, C. Johnson (2007). BioMesh3D: A meshing pipeline for biomedical models SCI Institute Technical Report UUSCI-2007-009, University of Utah.

[17] http://www.scirun.org; SCIRun

[18] R.Macleod, M.Janse, A. Oosterom, P.Kligfield, (2011), The forward problem of electrocardiography, Comprehensive Electrocardiology. vol. 1. Springer; p. 247-298.

[19] B.Buton, J.Tate, B. Erem, D.Swenson, D.Wang, R.McLoed, (2011), A Toolkit for Forward/Inverse Problems in Electrocardiography within the SCIRun Problem Solving Environment, Conf Proc IEEE Eng Med Biol Soc.pp: 267-270.

[20] https://www.sci.utah.edu/cibc.html

[21] H. Lim, W. Cun, Y. Wang, R. Gray, and J. Glimm (2018), The role of conductivity discontinuities in design of cardiac defibrillation, Chaos, vol: 28, 2018.

[22] O. Mazumder, D. Roy, S. Bhattacharya, A. Sinha, and A. Pal, (2019), Synthetic ppg generation from haemodynamic model with baroreflex autoregulation: a digital twin of cardiovascular system, IEEE Engineering in Medicine and Biology Society (EMBC). IEEE, pp. 5489-92.

[23] O. Mazumder, D. Roy and A. Sinha (2020), In Silico Cardiac Model to Evaluate Myocardial Ischemia effect on Hemodynamic Parameters, 28th European Signal Processing Conference (EUSIPCO), Amsterdam, pp. 1105-1109.

[24] R.Gilbert, M.Goldberg and J. Griffin (1954); Circulatory changes in acute myocardial infarction. Circulation; vol: 9, pp 847-54.

[25] William B. White (1999), Heart rate and the rate-pressure product as determinants of cardiovascular risk in patients with hypertension, American Journal of Hypertension, vol:12(22),pp: 50-55.